Minimum Induced Drag for Wings with Spanwise Camber

Martin V. Lowson*
University of Bristol, Bristol, England, United Kingdom

Linear theory is used to develop optimum circulation distributions and their associated minimum induced drag for wakes from lifting surfaces with various spanwise camber. The work is largely computational and results for cases previously investigated analytically are generally in good agreement. However, some previously published results are found to be in error, and a new solution for the induced drag of a wing with dihedral is given. New results are computed for polynomial and superelliptic camber lines. An empirical correlation is demonstrated between the induced drag factor and the inverse arc length for a variety of optimum cases.

Nomenclature

a = wing half length, $= s/\cos\beta$
b = ratio of the maximum amplitude of the camber divided by semispan
k = induced drag factor
M' = dimensionless added mass
s = semispan
v = induced velocity normal to the lifting line
w_0 = an arbitrary constant
β = local dihedral angle of the lifting line

Introduction

In recent years there has been a resurgence of interest in the idea of reducing the induced drag component of an aircraft by wing design. The most well-known example of recent work in this field is that of Van Dam[1] on planform modifications that suggests the use of wings with highly swept tips. The published work gives little detail of design methodology but relies on a panel method for analysis. Other panel methods are known to be problematic for induced drag prediction. This, and other methods, have been calibrated by their ability to predict an induced drag factor of 1 for the elliptically loaded wing case, the classical result of lifting line theory.

It is rather surprising that there has been little recent attempt to establish the extended predictions of lifting line theory for minimizing induced drag. Since the original work of Munk,[2] it has been known that spanwise camber can have significant effects in drag reduction. It is, thus, of interest to make a general study of the effects of spanwise camber on induced drag. Previous studies have been essentially analytic, and, although these have given much valuable insight, they have not had the flexibility to study general camber lines. A computational approach that permits greater flexibility in the definition of the camber line is indicated.

Such work has additional interest because the effect of planform on a lifting line model can be regarded as an in-plane curvature. At angle of attack, the effect of this curved lifting line is to cause a spanwise camber distribution. This seems to have been first suggested by Hoerner,[3] and Burkett[4] has recently noted that application of the Munk stagger theorem to this case permits the problem of planform optimization to be restated as a problem in the optimization of a wing with spanwise camber. There are formal difficulties with this concept of planform-camber equivalence since lifting line theory and the Munk optimization are based on linearized Trefftz plane analyses of the shed wake. The relation of the shed wake shape to the wing planform distribution remains unclear; for example, the actual shed wake shape at the trailing edge of the wing is not the same as the quarter chord condition normally assumed. It may be noted that this objection is also true for the relation of the optimum elliptic loading to the classic elliptic planform. Nevertheless, the concept of planform-camber equivalence appears to provide a useful empirical insight and suggests that study of spanwise camber can also give indications of potentially favorable planform shapes for reduced induced drag.

Approach

The present work inevitably starts from the Munk[2] results, which define the downwash velocity distribution required for optimum lift for a given camber. Munk's results may be written as

$$v = w_0 \cos\beta \tag{1}$$

Munk's results have consequences that do not appear to be well known, although they are not claimed to be new. In particular, it may be shown that under optimum conditions the ratio of lift to induced drag is constant at all sections along the wing. The consequence of this, in combination with the cosine condition [Eq. (1)], on a cambered wing is to reduce the lift (and induced drag) toward the tip of the wing under optimum conditions. In particular, the cosine condition requires that a vertical endplate, which has no vertical component of lift, also forces an optimum vorticity distribution that gives no induced drag anywhere on the endplate.

It may also be noted that all the results from the present linearized theory are symmetric in camber; i.e., positive camber gives identical benefits in induced drag to negative camber. Nonlinear effects, for example, tip separation and vortex rollup, would provide strong departures from this symmetry. The implication for planform is that under linear conditions forward sweep gives similar effects on induced drag to rearward sweep, a result also indicated in recent experimental work by Palmer.[5]

For the present results, the lifting line is replaced with a series of horseshoe vortices describing the bound and shed vorticity but permitting a prescribed spanwise shape. The mathematics for this follows the classical techniques for description of vortex sheets and does not justify detailed description here. The general approach is to break up the shed vortex sheet into a number of elements, to compute the locally induced velocity and, thus, local forces at intermediate collocation points on the lifting line, and to invert the resulting matrix to determine the vorticity distribution, which satisfies the Munk optimum downwash criterion.

Received Nov. 30, 1989; revision received Feb. 9, 1990.

*Professor, Department of Aerospace Engineering. Associate Fellow AIAA.

Table 1 Effect of number of collocation points on the calculated value of the induced drag factor k

Number of points	10	20	40	60	100	∞[a]
Uncambered	0.999999	1.000000	1.000000	1.000000	1.000000	1.000000
Semicircle	0.649323	0.657969	0.662309	0.663764	0.664927	0.666671

[a]Calculated by a polynomial projection of the results for 60 and 100 collocation points.

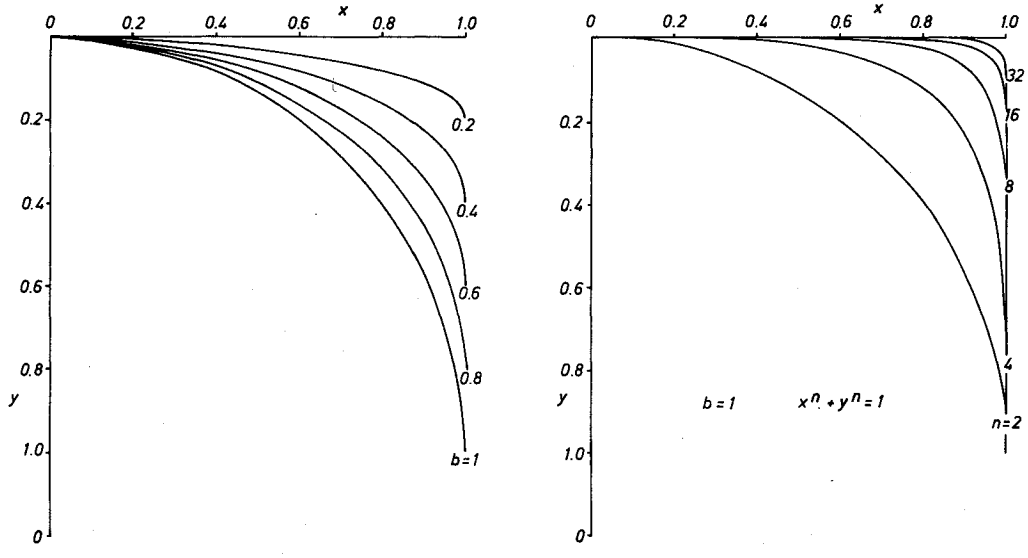

a) Elliptic b) Superelliptic

Fig. 1 Wing shapes.

The crucial issues are the distribution of shed vortex elements on the lifting line and the choice of collocation points to provide satisfactory convergence. All the computations were performed on a personal computer, which permitted a maximum number of vortex elements of 100. Poor choice of calculation points resulted in poor convergence, and much of the work has been associated with finding initial distributions of vortex locations and collocation points that gave good convergence in the solution.

For conventional wings, the "Weber points" established by J. Weber of the Royal Aerospace Establishment (RAE) (see Ref. 6) are known to give good convergence. These require distributing the vortex elements in an inverse cosine distribution along the lifting line, found by striking verticals to the diameter from a uniform angular distribution around a circle. Collocation points are found by the same process at the points distributed at the semiangle intervals around the circle.

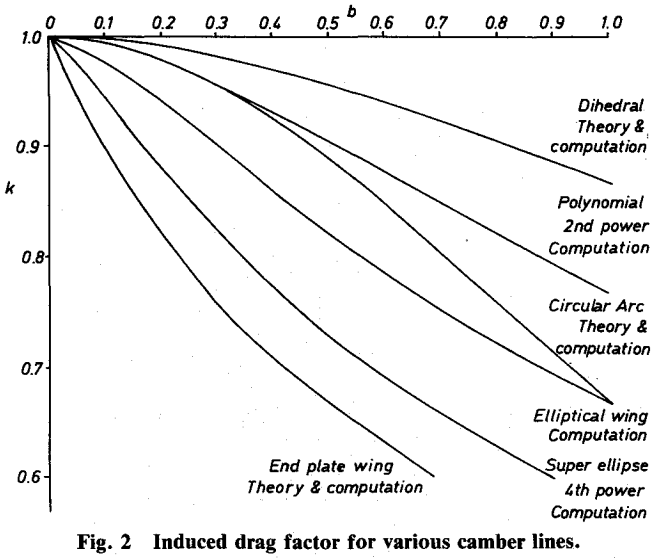

Fig. 2 Induced drag factor for various camber lines.

Use of these points for the calculation gave good results for more conventional cases, such as the straight lifting line and circular arc. Examples of convergence are given in Table 1. It can be seen that good comparison with known analytic solutions, i.e., one for the straight line and two-thirds for the semicircular arc, can be achieved for small numbers of vortex elements.

If convergence is found, then a more accurate solution can be determined by extrapolation of the trend with increasing number of vortices to infinity. This corresponds to a projection using a polynomial in powers of $1/n$. Typically, a first-order projection using two results is sufficient. The results of such projections are also shown in Table 1 for an extrapolation to infinity of the results for 60 and 100 vortices. It will be observed that, even for the demanding case of the semicircular arc, results to five figure accuracy can be obtained. All the results presented in this paper use this extrapolation method, and are based on a maximum number of vortex points of 100.

The accuracy of the results was found to be extremely sensitive to fine detail of the vorticity distribution at the tip. It is intriguing that experimental results are also sensitive to such effects with local separations near the tip having a significant role. The Weber points give a much increased density of points near the tip, and this accounts for their general accuracy. However, shapes with stong spanwise camber near the tip were found to require a still higher tip vortex density. A number of essentially empirical methods were developed to provide suitable distributions, which were judged satisfactory when convergence with increase of number of calculation points was consistent.

Results

Initial Results and Comparison with Previous Work

A wide variety of shapes has been investigated in the present work. Some of these are shown in Fig. 1. The results from several of the computations of induced drag for these wing shapes are compared in Fig. 2. Note that the induced drag factor k is defined following European practice, by

$$C_{DI} = k\, C_L^2 / \pi \mathcal{R} \qquad (2)$$

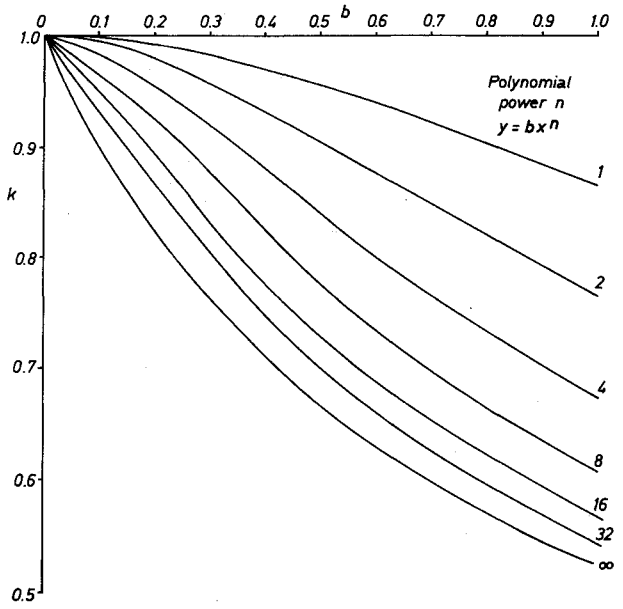

Fig. 3a Induced drag factor, polynomial camber.

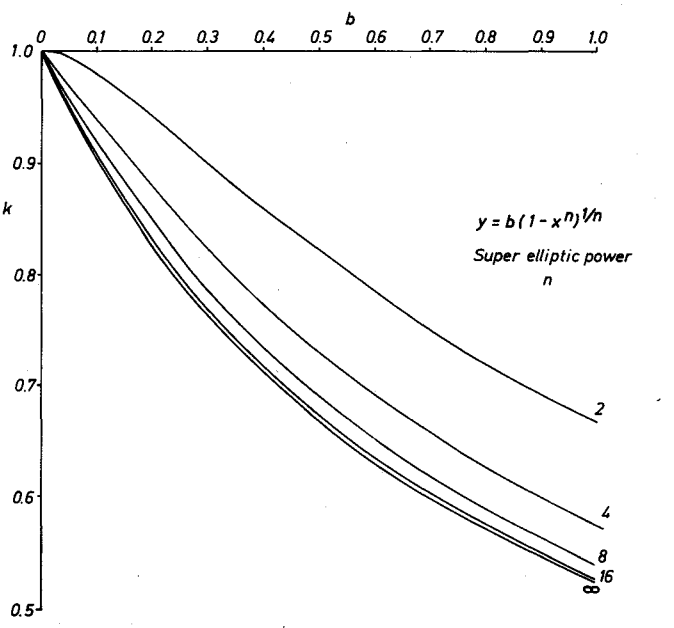

Fig. 3b Induced drag factor, superelliptic camber.

Thus, values of $k < 1$ imply reductions of induced drag.

There are several known analytic solutions to the optimum spanwise camber problem, for example, the circular arc wing[7] and the wing with end plates.[8] The computational results have been compared with these known analytic solutions, in particular with the circular arc wing, for which Cone[7] gives the formula in the present notation:

$$k = (1 + 0.5\, b^2)^{-1} \tag{3}$$

Comparison of the computations, including the extrapolation method discussed above, with this formula gave better than five figure accuracy in induced drag in every case (see Table 1). In general, it is believed that at least four figure accuracy has been maintained in the cases reported in the present paper.

Results were also computed for the wing with an end plate. In this case, the Weber point distribution was extended down the end plate of the wing. These results showed adequate agreement with those indicated by Mangler.[8] It is thought that the divergencies, which were small and unsystematic, were probably due to difficulties in measurement from the small graphs on which the data were presented.

However, comparison of the computational results with some of the previously published cases did give rise to systematic disagreements. It has been found that some of the published results in the literature are numerically incorrect, in particular, those for the elliptic camber distribution given by Cone[7] and for the wing with dihedral given by Letcher.[8]

In the case of the wing with elliptical camber distribution, the reason for the disagreement seems straightforward. Although Cone used analytic techniques to produce the majority of his results, the elliptic wing cases were calculated via an analog method using Teledeltos electrical plotting paper. It seems clear that those results were less accurate than hoped at the time, and the present results for elliptic camber lines may be taken as more representative.

This point has been discussed by Lundry and Lissaman,[10] in work on nonplanar wings with pylonlike panels. They pointed out that Cone's results were measured on plotting paper of finite size so that the boundary conditions were incorrect. They also suggested that the results could be modified following wind-tunnel correction techniques.

Wing with Dihedral

The comparison of the results with those of Letcher for the wing with dihedral showed a modest but significant variation from his published data, typically in the third significant figure. Letcher gives an explicit integral formula for the added mass of the dihedral wing, which can be written as

$$M' = (1 - \alpha)/\alpha^2, \qquad \alpha = 0.5 - \beta/\pi$$

$$a(\alpha) = \int_0^1 \Big/ \left(\frac{1-\alpha}{\alpha+\xi}\right)^{-\alpha} \tag{4}$$

This result for added mass is directly relevant to the slender wing case, and is related to the induced drag factor by the formula

$$k = \cos^2\beta / M' \tag{5}$$

The integral in Eq. (4) has an integrable singularity at $\xi = 1$ that makes numerical evaluation awkward. The integral was recalculated using an analytic technique to ensure proper convergence at $\xi = 1$, and the results agreed closely with the present fully computational approach. It was therefore concluded that Letcher's numerical results were inaccurate.

It was also observed that the recomputed result for the case $b = 1$, i.e., $\beta = \pi/4$, $\alpha = 0.25$, gave an added mass of $\sqrt{(1/3)}$ and an induced drag factor of $\sqrt{(3/2)}$ to better than seven figures. (Letcher's result was $M' = 0.575$, giving $k = 0.868$.) This numerical observation motivated further studies.

By changing the variable of integration to $x = (1 - \xi)$, it is possible to determine an explicit series solution to the integral in Eq. (4), which was used in early parts of the present work. However, recently J. H. B. Smith of RAE Farnborough has been able to find an explicit analytic solution to the integral in Eq. (4), which is

$$a = [(1 - \alpha)/\alpha]^{1-\alpha} \tag{6}$$

This result gives further formulas for the added mass and induced drag factors for the wing with dihedral as

$$M' = [(1 - \alpha)/\alpha]^{2\alpha - 1} \tag{7}$$

and

$$k = \cos^2\beta [(1 - \alpha)/\alpha]^{1-2\alpha} \tag{8}$$

These equations give results in close agreement with the previously computed results and also confirm the result for $b = 1$ found computationally.

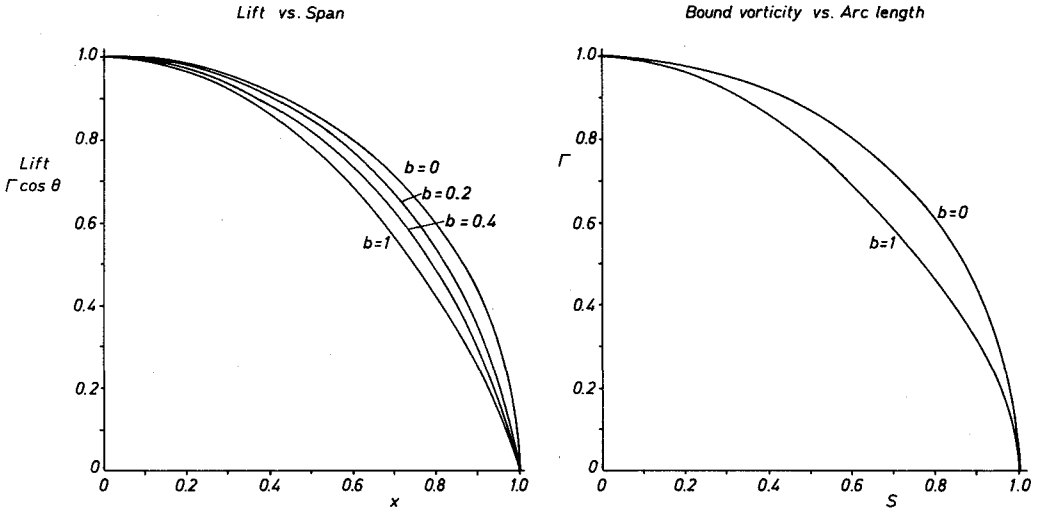

Fig. 4a Lift and vorticity distribution, elliptic camber.

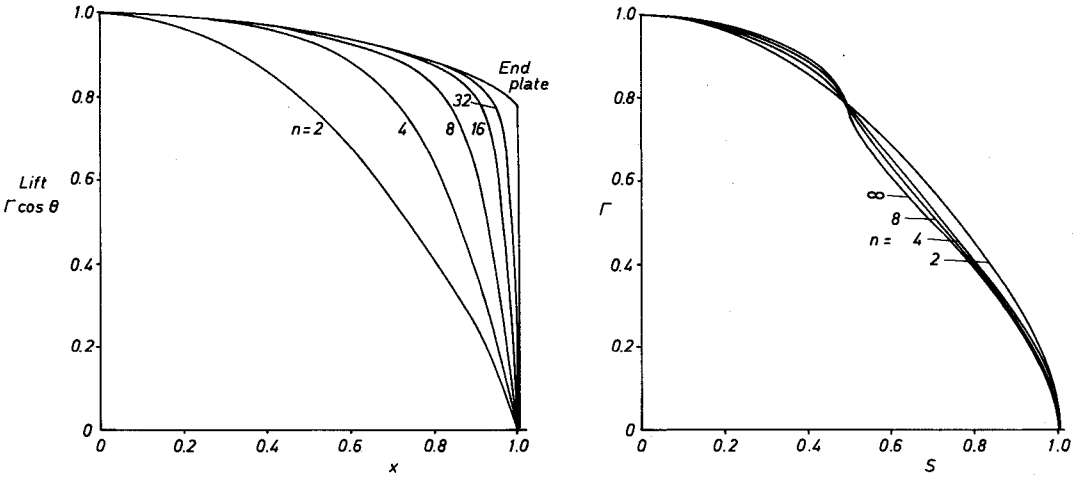

Fig. 4b Lift and vorticity distribution, superellipse $b=1$.

Additional Results

Having established the effectiveness of the computational procedures, it was thought of interest to evaluate two additional families of spanwise camber. The first was a simple polynomial shape of form $y=x^n$. A set of curves giving the results is presented in Fig. 3a.

The second family to be studied was based on the superellipse given by $y^n+x^n=1$. The results for this family are shown on Fig 3b. It will be observed that the superelliptic results give low values of k and therefore may be of some practical interest.

Lift and Vorticity Distributions

The computational procedure automatically provides lift and vorticity distributions for each case. Only representative results are given here. For each case, plots are given of lift against wing semispan and of bound vortex strength against wing arc length.

Figure 4a gives results for a characteristic case of the elliptic camber wing for a range of values of b. At $b=1$ the ellipse becomes a circular arc of equal semispan and out of plane height. In Fig. 4b, results are given for the superelliptic wing for a value of $b=1$, but for various values of the exponent n. As n increases, the superellipse tends toward a wing with endplate; computed results from this case are also shown for comparison.

Discussion

Figure 2 gave a summary of the results for minimum induced drag for various shapes of lifting line. There is a strong effect of spanwise camber distribution on induced drag. Comparison of the results for various shapes demonstrates that it is the shape of the tip and, in particular, its vertical orientation that is the principal factor governing the benefits. For any given value of b, the maximum reduction of induced drag is always found for the simple end plate. The superelliptic case provides a family that systematically approaches the end plate form as the exponent is increased. Quite modest superelliptic exponents give results close to the end-plate case. The polynomial curves are essentially equivalent in shape to the superelliptic cases over the inboard part of the wing for the same value of exponent but differ noticeably near the tip. The major difference in induced drag factor confirms the strong effect of the tip shape. The same conclusion can be drawn by comparing the circular arc and elliptic cases.

The results for lift and vorticity distributions presented in Fig. 4 are representative of the results obtained during the work. For all cases with modest camber, the distributions were close to elliptic, particularly when considered in terms of bound vorticity vs arc length. This result is not unexpected. Figure 4b shows the distribution as the wing changes from circular to square arc form. The results show how the optimum distributions over the parts of the wing that are superposed in form (see Fig. 1) are also superposed. The variation from the elliptic distribution is less when considered in terms of bound vorticity vs arc length.

The results also showed that total arc length of a cambered wing was a strong empirical predictor of induced drag. Figure 5 gives a plot of k^{-1} against total arc length for various wing shapes. The arc length and inverse drag factor are closely

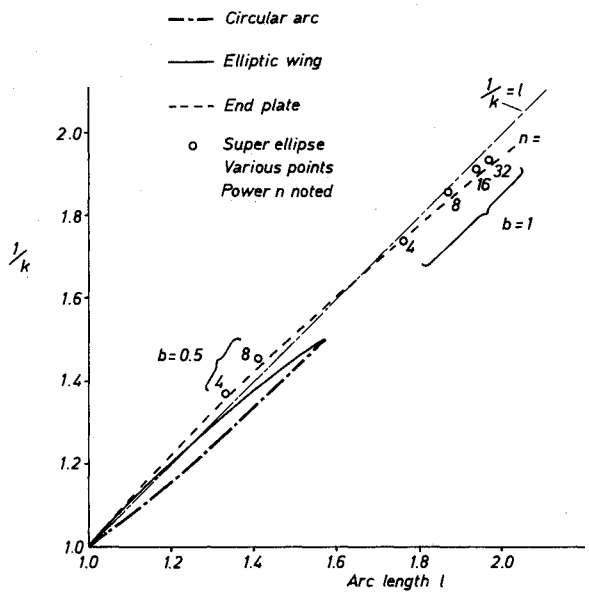

Fig. 5 Correlation of induced drag factor and arc length.

related for the more effective wing forms such as end plates, superellipse, etc. For wing forms without vertical tips, the correlation is less strong, but there is still a strong empirical trend. The most effective form for a fixed arc length is a broadly elliptic shape of modest overall camber.

However, it will be recalled that the induced drag is proportional to the inverse square of the span, so that the best use of arc length is generally to increase the span rather than to use camber. One exception to this is the use of spanwise sweep, which gives no additional wing span, but which does provide an effective "free" spanwise camber at incidence via the planform-camber equivalence noted in the Introduction.

It is, therefore, also of interest to examine the consequences of these results on planform. They suggest that changes in the planform distribution toward the tip would have the strongest effects, as already indicated by the results of Van Dam.[1] The present results give a prescribed downwash and bound vorticity distribution for minimum induced drag under the assumptions of the linearized theory. However, as discussed in the Introduction, they cannot give explicit suggestions for planform distributions without further assumptions about the consequences of planform on downwash. Direct application of the planform-camber equivalence principle at cruise angle of attack through consideration of quarter-chord distribution only leads to small values of b, around 0.05, for even quite substantial planform sweeps. This would give a maximum induced drag reduction at cruise of around 3–4% compared with the Van Dam[1] predictions of up to 10%. However, the results also suggest that benefits of 10% or more could be available from planform at higher incidences; this could be of value to the designer.

Previous recent work has emphasized the nonlinear distortion of the vortex sheet as the principal feature of the planform effects on induced drag. Although such effects are unquestionably important, the present results show useful insights from a linear analysis. The results are put forward as a contribution to design of wings of reduced induced drag and offer a variety of model cases for further investigation in the same way as the original lifting line theory provided the basic elliptic wing.

Conclusions

Computation of optimum lift distributions for cambered lifting lines has shown that the benefits are largely due to camber near the tips. The most effective form of camber for a given maximum displacement is the end plate, but elliptic and superelliptic shapes are slightly more effective in terms of minimum length of wing for a given displacment.

More accurate results have been presented for the wing with elliptic camber and the wing with dihedral. The new results for polynomial and superelliptic wings may have some practical interest. The principle of planform-camber equivalence offers a method of exploiting these results to provide suggestions for new planform designs.

Acknowledgments

I would like to thank C. W. Burkett for starting my interest in this problem and S. P. Fiddes for his advice during the work.

References

[1]Van Dam, C. P., "Induced-Drag Characteristics of Crescent-Moon-Shaped Wings," *Journal of Aircraft*, Vol. 24, No. 2, 1987, pp. 115–119.

[2]Munk, M. M. "The Minimum Induced Drag of Aerofoils," NACA Rept. 121, 1921.

[3]Hoerner, S. F., *Aerodynamic Drag*, Hoerner, 1953.

[4]Burkett, C. W., "Reductions in Induced Drag by the Use of Aft Swept Wing Tips," *Aeronautical Journal*, Vol. 93, 1989, pp. 400–405.

[5]Palmer, M.E. "Drag Development at Low Speeds on Forward Swept Wings," Univ. of Bristol, Bristol, England, Rept. 402, 1990.

[6]Thwaites, B. (ed), *Incompressible Aerodynamics*, Oxford University, Oxford, England, 1960, p. 136.

[7]Cone, C. D. "The Theory of Induced Lift and Minimum Induced Drag on Non-Planar Lifting Systems," NASA TR-R-139, 1962.

[8]Mangler, W., "The Lift Distribution of Wings with End-Plates," NACA TM-856, 1938.

[9]Letcher, J. S., "V-Wings and Diamond Ring Wings of Minimum Induced Drag," *Journal of Aircraft*, Vol. 9, No. 8, 1972, pp. 605–607.

[10]Lundry, J. L., and Lissaman, P. B. S., "Minimum Induced Drag on Non-Planar Wings," *Journal of Aircraft*, Vol. 5, No. 1, 1968, pp. 17–21.